ISSN 2616-5880 Vol. 4, Issue 5: 61-70, DOI: 10.25236/AJMC.2023.040509

Storage Characteristics and Mechanism of Organic Small Molecule Charge-Capturing Materials Based on Electric Field Force Microscopy

Wenjie Jiao, Xu Wang*

School of Materials Science and Engineering, Yancheng Institute of Technology, Yancheng, Jiangsu, 224000, China
13675267884@163.com
**Corresponding author*

Abstract: *As people's living standards become higher and higher, the requirements for computer technology are becoming more and stricter, including the storage performance of computers is particularly demanding. However, there is currently no suitable method for effectively analyzing the storage performance of a computer. In order to carry out in-depth and effective research on the charge storage performance of the memory, based on the working principle of electric field force microscopy, a detailed analysis of the organic small molecule material, polyvinylpyrrolidone (PVP), was carried out by constructing a molecular dynamics model. It turns out that PVP exhibits different characteristics at different temperatures. We can think that the extremely low temperature rise is beneficial to improve the storage performance of storage components, but it cannot exceed 360K. The paper also analyzes the aging properties of the charge. It is found that the stored charge in the device has good time-lasting performance. At the same time, the capacitance value of the film changes with time and has very small fluctuations, showing a very stable property. This shows that the loss of charge is very small and has good charge aging properties.*

Keywords: *Electric Field Force Microscope, Polyvinylpyrrolidone (PVP), Storage Sharge, Aging Properties*

1. Introduction

With the rapid development of science and technology and culture in the 20th century, a large number of Numbers, words and pictures need to be stored, and the traditional memory can no longer meet People's Daily needs. Therefore, finding a more convenient, efficient, safe and reliable memory has become the primary task of scientists. At present, much traditional non-volatile memory can’t meet the requirement of miniaturization. As a new type of memory, charge capture memory is considered to be a new generation of non-volatile memory with great application prospect. Organic small molecule materials have good electrical properties, which provide an opportunity for the development of charge capture memory.

In this paper, electric field force microscopy (SEM) was used to propose a molecular dynamics model based on charge trapping. The charge transport properties of PVP films were studied. The substrate temperature was obtained by calculating the charge mobility of PVP at different substrate temperatures. A reasonable range. In order to compare the effects of pre- and post-Ge on the electrical and storage properties of PVP films. Under the same preparation conditions, the authors deposited the same thickness of Ge-doped and Ge-doped PVP on the same PVP substrate and carried out comparative analysis.

Section 1 is the introduction, which provides an overview of the overall structure of the article. Section 2 is a review of relevant literature on electric field force microscopy and charge storage performance at home and abroad. Section 3 is the experimental model and related theoretical methods used in the article. Section 4 is the experimental part, including the preparation and evaluation criteria of the experimental materials. Section 5 is the analysis and discussion of the experimental results. Section 6 is a summary of the article.

ISSN 2616-5880 Vol. 4, Issue 5: 61-70, DOI: 10.25236/AJMC.2023.040509

2. Related Work

Whether it is organic or inorganic materials, its electrical properties have a huge impact on the storage performance of electronic memories, so many researchers have studied the electrical properties of various materials. In [1], the authors prepared a 3, 4, 9, 10-dianhydride (PTCDA) doped polymer film by solid solution method using polypyrrole (PPy) and polyvinyl alcohol (PVA) as raw materials. The uniform morphology of the sample with high PTCDA mass fraction was studied by atomic force microscopy (AFM). The conductivity response of the polymer organic semiconductor was determined by impedance spectroscopy. The results showed that the highest DC conductivity (2.08×10 -3 S/m) was obtained for 10 wt% of PTCDA at 1400C.In [2], the authors studied the photoelectric property modulation of single crystal nanorod arrays of per-3,4,9,10-tetracarboxylic dianhydride (PTCDA). This study proves that, unlike PTCDA films, PTCDA nanorods have optical waveguide characteristics in the visible region. The electrical properties of PTCDA nanorods show that the conductivity along the growth direction of nanorods is about 0.61 S·m-1. Higher than the conductivity of pure crystalline PTCDA film. The photoelectric property modulation of the single crystal sample contributes to the improvement of the quality of the single crystal product. In [3], the topological structure and electronic structure of two-dimensional PANI are revealed by the author by means of microscope and spectroscopy combined with first-principle density functional theory. The electronic properties of the original two-dimensional PANI film showed bi-polar behavior, with a Dirac point of -37v and an average conductivity of 0.72 S/cm. After adding hydrochloric acid, the conductivity jumps to 1.41×103 S/cm, which is the highest conductivity of PANI doping at present. In [4], the authors studied the electrical properties of organic and non-polar semiconductors doped with molecules, and revealed that one of the major differences between inorganic and organic semiconductors is their respective electron state density and doping-induced changes. In organic semiconductors, the coulomb attraction between ionized dopants and free-charge carriers is usually stronger due to its lower dielectric constant. In [5], the authors studied the electrical properties of Zn1-xCa x O (x = 0, 0.01, 0.02 and 0.03) nanoceramics synthesized by solid-state reaction from room temperature to 5000C using complex impedance spectroscopy (CIS). The structure of the composite material was analyzed using X-ray diffraction techniques. The experimental results show that the dielectric constant of the material decreases with increasing frequency and temperature of the Ca-doped sample. The dielectric loss of Ca-doped ZnO samples at low temperatures is lower than that of pure ZnO. In [6], the holes transport and electrical characteristics of small molecular organic materials commonly used in organic light-emitting diodes were studied. The results show that without carrier density and electric field dependence, the traditional mobility model can't well describe the relationship between current density and voltage (j-v) of holes devices. In addition, it is proved that boundary carrier density has an important effect on j-v characteristics. The maximum carrier density and the minimum electric field appear near the interface of NPB pure holes devices. In [7], the photoelectric properties of organic metal halide perovskite materials were studied. The study outlines the relationship between the composition and morphology of the material and the photoelectric properties of the material and how these properties ultimately affect the performance of the device. The properties of different perovskite materials are analyzed, and the parameters such as band gap, mobility, and diffusion length and carrier life are studied. This research contributes to the wide application of organometrics halide perovskite in the field of optoelectronics. In [8], the author studied the rectification behavior and performance parameters of organic/inorganic hybrid polycompounds, studied the characteristics of organic layer and inorganic layer, realized the heterogeneous junction between organic layer and inorganic layer, and optimized the heterogeneous junction. The threshold voltage of the optimized heterogeneous junction (thickness ~ 600nm) is 0.4v, with rectification characteristics, and the ideal factor is lower (n ~ 1.6), which can reduce current leakage. To sum up, scholars at home and abroad have made fruitful researches on the electrical properties of many materials, but there are also some problems: there are few researches on the electrical properties of materials from the microscopic aspects such as charge capture and charge diffusion; There is a lack of understanding on the photoelectric properties of organic semiconductor materials at the nanoscale.

In [9], the authors point out that atomic force microscopy (AFM) and other microscopic techniques are becoming basic tools for in-depth study of morphology and structural characteristics at the micro and submicron scales to evaluate the time relationship between physical and chemical properties of biological materials and biological reactions. AFM is not only a tool for screening surface morphology, but also an important contribution to understanding surface and interface properties to optimize the properties, processes, physical and chemical properties of biomaterials at the micro and nanoscale. It is possible to apply the latest discoveries in nanotechnology to soft materials, such as atomic force spectra, which measure surface forces by force curves. Information such as elasticity, viscoelasticity, surface

ISSN 2616-5880 Vol. 4, Issue 5: 61-70, DOI: 10.25236/AJMC.2023.040509

charge density and wettability can be collected by local interaction of samples. In [10], the author used kelvin probe force microscope (KPFM) to characterize its interface by cross-sectional area of a-si: H. The section area of the a-si: H cracking sample was obtained by mechanical cold polishing. This study used nanoscale resolution to measure the contact potential difference of the cross-sectional area of a-si: H. Therefore, electric field force microscope can be used to study the electrical properties of organic small molecular materials [11].

3. Method

3.1. Operating Principle of Electric Force Microscope

When there is a charge on the sample, there is a long-range electrostatic force between the probe and the sample. In order to separately detect the long-range electrostatic force and eliminate the influence of other forces between the probe and the sample (van der Waals force and damping force, etc.), the AFM probe can be raised to a certain height relative to the surface of the sample, so that the probe is away from the surface of the sample, only the role of long-range electrostatic forces. This mode of operation is called the lift mode [12]. EFM is working in lift mode. In the lift mode, the probe first sweeps a line back and forth across the surface of the sample, performs a topographical image, and records the contour profile here. Then, along the strip profile curve, a certain height is raised (generally tens to more than 100 nanometers) for long-range electrostatic force detection, thereby obtaining a phase diagram reflecting the electrical properties of the sample. Under the action of long-range electrostatic force, the resonance peak of the probe is shifted, and the magnitude of the long-range electrostatic force can be reflected by collecting the phase change of the probe vibration [13]. Of course, although the phase diagram obtained by EFM is a quantitative result, it does not directly represent the absolute value of long-range electrostatic force. Therefore, EFM is usually used as a qualitative study of the surface charge distribution of a sample. To perform a quantitative charge calculation, a corresponding model must be established for different sample systems. The phase diagram obtained in EFM mode reflects the relationship between the probe and the sample. When the EFM is performing electrical measurements, the probe is in an electric field excited by the charge, so there is a potential difference between the place where the charge is present on the sample and the probe. If a voltage V is applied between the probe and the sample such that the potential difference is zero, then the probe is subjected to a long-range electrostatic force of zero and the probe motion state remains unchanged. At this point, the applied voltage V is related to the surface potential on the sample. If the voltage V is presented as a result, then the surface potential of the sample is reflected. EFM is primarily used to characterize changes in the electric field force gradient at the surface of a material. In general, the change in the electric field gradient is caused by the field source, which can be either the trapped charge in the material or the voltage applied to the material. In our experiments using EFM to characterize the charge storage capacity of materials, the charge captured by the material acts as the field source at this time, and the process of charge diffusion is the process of changing the field source. The charge diffusion can be monitored by applying a reasonable amount of voltage to the tip to measure the change in the electric field force gradient on the surface of the material, characterizing the change in the electric field force gradient on the surface of the material [14].

3.2. Molecular Dynamics Model Based on Charge Capture

(1) Molecular force field

Different potential energy terms are expressed in different forms. The most common form of system potential energy function with N atoms is:

$$U=\frac{1}{2}\sum_i k_b\left(l_i-l_i^0\right)^2+\frac{1}{2}\sum_i k_\theta\left(\theta_i-\theta_i^0\right)^2+\frac{1}{2}\sum_i V_i(1+\cos(n\phi-\gamma))+\sum_{n=1}^{N-1}\sum_{n=m+1}^{N}\left(4\varepsilon_{mi}\left[\left(\frac{\sigma}{r_{mn}}\right)^{12}-\left(\frac{\sigma}{r_{mn}}\right)^{6}\right]\right)+\sum_{m=1}^{N-1}\sum_{n=m+1}^{N}\left(\frac{q_m q_n}{4\pi\varepsilon_0 r_{mn}}\right) \quad (1)$$

Among them, the first term is the key expansion potential energy term, where the most common mode of harmonic vibration is given, kb is the elastic constant, and li and li0 are the instantaneous bond length and balance bond length of the i-th key; Is the bond angle bending potential energy, the form and the key expansion potential energy belong to the simple harmonic vibration; the third term is the dihedral angle distortion potential energy, the form is related to the expanded series n; the fourth term is the non-bonding potential energy, given in the formula It is the most common form of expression of Lennard-Jones (LJ) potential energy, also known as 12-6 potential energy, rmn is the distance between

ISSN 2616-5880 Vol. 4, Issue 5: 61-70, DOI: 10.25236/AJMC.2023.040509

atoms m and n; the fifth term is the Coulomb electrostatic potential energy, and q is the charge carried by the atom.

(2) Numerical solution of Newton's equation

The position function of the particle is usually expanded in Taylor form as shown in the following equation:

$$v(t) = \frac{dr}{dt} = \frac{1}{2\delta t}[r(t+\delta t) - r(t-\delta t)] \tag{2}$$

That is to say, the position at time t+δt can be predicted by the position of t-δt and t, and then the velocity at time t can be obtained by the position at time t-δt and t+δt. However, as can be seen from the equation, there is a truncation error in the calculation of the position, and as the number of calculations increases, the cumulative error will gradually increase. Moreover, there is no speed term in the equation. Considering that the speed term is related to kinetic energy, the kinetic energy is determined by the system temperature, so this will cause the position to be unrelated to the system temperature. Rearrange the position expression to get [15]:

$$r(t+\delta t) = r(t) + \delta t\left[v(t) + \frac{1}{2}a\delta t \right] = r(t) + v\left(t + \frac{1}{2}\delta t \right)\delta t \tag{3}$$

On the basis of knowing $v\left(t - \frac{1}{2}\delta t \right)$ and r(t), the acceleration a(t) can be obtained by the position r(t) at time t, and then the velocity $v\left(t + \frac{1}{2}\delta t \right)$ at time $t + \frac{1}{2}\delta t$ can be obtained by the above formula, and the velocity at time t is also can be obtained by the above, and so on.

3.3. Storage Characteristics Research Model Based on Electroluminescence Theory

(1) Charge transfer of molecules

In the process of electron transfer, the transfer of energy is accompanied by the transfer of excited state energy. Energy transfer can occur between molecules or within molecules. For the energy transfer between molecules, it can be the same energy transfer between molecules, or energy transfer between different molecules; energy transfer inside the molecule refers to two or a few in the same molecule. Energy transfer between chromophores, these chromophores may be the same or different. According to its nature, energy transfer can be divided into two categories: radiation transfer and non-radiative transfer [16]:

1) Radiation energy transfer: For example, the transfer of radiant energy between a donor and a receptor can be expressed by:

$$\begin{aligned} D^* &\rightarrow D + hv \\ hv + A &\rightarrow A^* \end{aligned} \tag{4}$$

Studies have shown that the probability of this energy transfer is related to the emission quantum efficiency of the excited state donor D*, the concentration absorption coefficient of the acceptor A, and the overlap of the emission spectrum of D* and the absorption spectrum of A, but independent of the medium concentration.

2) Non-radiative energy transfer: Unlike radiant energy transfer, the non-radiative energy transfer process is a one-step process:

$$D^* + A \rightarrow D + A^* \tag{5}$$

This requires that $D^* + D$ and $A^* + A$ have the same energy and require spin conservation.

(2) Molecular orbital theory

The electrons in the molecule move under the average potential field formed by each nucleus and other electrons. The motion state of the ith electron is described by the wave function ψi, which is

ISSN 2616-5880 Vol. 4, Issue 5: 61-70, DOI: 10.25236/AJMC.2023.040509

called the single electron wave function in the molecule, which the chemist calls molecular orbital. Ψi∗ψi is the probability density of i-space distribution in space. Ψi*ψidτ represents the probability that electrons are found at the micro-volume dτ near a certain point in space. The state of the entire molecule is dominated by the wave function of the electrons ψ1 × ψ 2 × ψi ... ψ n, and the energy is the sum of the molecular orbital energies of the respective electrons.

$$\psi = C_a\phi_a + C_b\phi_b \tag{6}$$

$$\hat{H}\Psi = E\Psi$$

Meet the Schrödinger equation: $\hat{H} = -\frac{\hbar^2}{2m}\left(\nabla_a^2 + \nabla_b^2\right) + V_a + V_b$. Through the above calculations and discussion, it can be seen that the orbits φa and φb can constitute the molecular orbitals ΨI and ΨII.

(3) Conductance of organic small molecular materials

The conductivity is expressed as: $\sigma = nq\mu$. Where n is the carrier concentration, q is the electron charge, and μ is the mobility. If there are 1 types of carriers in the material, then: $\sigma = \sum_{i=1}^{l} q_i n_i \mu_i$. From the characteristics of conductivity, the conductivity of organic materials can be divided into electronic conductivity σe and ion conductance σi, so there is: $\sigma = \sigma_e + \sigma_i$. In inorganic materials, ionic conductance is rarely discussed except for fast ion conductor materials, but for organic materials and polymers, various catalysts and stabilizers are added during synthesis or polymerization, and often at high temperatures. Since it is carried out, an organic material such as a polymer contains a considerable ionic component and various ionic decomposition products. There are therefore varying degrees of electronic conductance and ionic conductance in the polymer.

4. Experiment

4.1. Experimental Data

(1) Preparation of polyvinylpyrrolidone (PVP)

This experiment used k30 PVP powder with a molecular weight of 40,000 produced by Anhui Haifeng Fine Chemical Co., Ltd. First, 8g of PVP powder was dissolved in 50 ml of distilled water, and stirred for 30 minutes to completely dissolve PVP. The solution was a pale yellow opaque solution. After standing for 1 hour, the solution was poured into a tetrafluoroethylene film plate placed on a horizontal surface, and allowed to stand for one week to obtain a PVP film having a thickness of 120-160μm, and the PVP film was cut into a circular shape having a diameter of 12mm, and the double-sided plating diameter was 10mm conductive silver paste is used as electrode for pyroelectric and dielectric measurement.

(2) Preparation of organic small molecular materials doped with Ge oxide film

In order to compare the effects of pre- and post-Ge on the electrical and storage properties of PVP films. Under the same preparation conditions, the same PVP substrate was deposited to prepare Ge-doped Ge atoms and Ge-doped PVP. The prepared samples were annealed in high-purity N2 at 600°C for 30min, then on them. Covering a metal mask having a diameter of 0.2mm, DC sputtering a 150 nm thick electrode as an upper electrode, and finally preparing a lower electrode with silver paste to form an organic semiconductor capacitor structure.

4.2. Experimental Plan

(1) Experimental approach

In this paper, we will improve the reliability of the device by analyzing the thickness of the organic small molecule material and the materials participating in the process reaction through experimental methods. Data analysis was performed on the storage characteristics of organic small molecule materials, and improvements were made through analysis. From theory to practice, analyze and change the different important parameters that affect the storage characteristics of the device to find the best

ISSN 2616-5880 Vol. 4, Issue 5: 61-70, DOI: 10.25236/AJMC.2023.040509

method and solution.

1) Theoretically, the charge transfer mechanism of the two structures under the two conditions of erasing and writing is established, and the storage performance of the device is experimentally analyzed.

2) Compare the storage performance before and after improvement by using the comparative analysis method.

3) Actual testing and data analysis of the device.

(2) Experimental equipment

Infrared spectroscopy characterization: using Galaxy series 4030 infrared spectrometer, using Win FIRST V2.10 software, KBr crystal film formation method, the number of scans 64, the accuracy is 4 cm-1.

The nuclear magnetic resonance measurement was carried out on a NMR-FX290Q nuclear magnetic resonance apparatus using deuterated chloroform (CDCl3) as a solvent at a test temperature of 45°C and a number of scans of 100.

DSC analysis: Perkin Elmer's Pyris-1DSC60 differential scanning calorimeter, the heating rate is 10.0°C/min, the temperature rise range: 20.0 ~ 300.0°C.

Wide angle X-ray diffraction (WAXD) was measured by a Philips Dual X'Pert X-ray diffractometer.

The vacuum coating equipment is a DM-200 high vacuum coating machine produced by Shanghai Xinyue Instrument Factory. Under a vacuum of 6.67×10-3Pa, double-sided aluminum plating is used as an electrode. The surface resistance of the aluminum film is less than 2 ohms.

The pyroelectric measurement is carried out on the improved thermoelectric analyzer produced by Toyo Seiki Co., Ltd., and the measurement accuracy can be higher than 10-13A, the input impedance is higher than 1012Ω, and the data acquisition and temperature control are realized by microcomputer joint control. For detailed measurement steps, see Chapter 1, Pyroelectric Overview. The pyroelectric theory fitting program is a DOS program compiled by the laboratory. Usually, the polarization field strength of the sample is Ep=20k V/cm, the polarization time is tp=10min, and the temperature rise rate of the TSDC test is 4°C/min.

4.3. Evaluation Indicators

(1) Polarization of organic small molecular materials

A circular electrode having a diameter of 1.5cm and a thickness of 100nm was vapor-deposited on one side of the sample before the electret. When the pole is poled, the side plated with the electrode is grounded. The electret conditions are: the distance between the needle electrode and the sample surface is 4 cm; the needle voltage is -8 kV; the electret time is 5min. The environmental conditions are room temperature 25°C, atmospheric pressure 760mmHg; relative humidity 45%. Post-elected samples are stored in a desiccator to reduce charge decay caused by air ions. The function of the gate control is to evenly distribute the space charge trapped in the sample, and at the same time effectively control the charge density of the sample. If the gate is filled with a gateless corona, the surface potential distribution is extremely uneven, and it is distributed in a bell shape in the radial direction (that is, the surface potential at the center of the sample is significantly higher than the surface potential around it).

$$\frac{i}{i_{\max}} = \left(1 + \frac{r^2}{l^2}\right)^{-5/2} \tag{7}$$

Where r is the distance from the point to the center of the sample, l is the distance from the tip to the sample, and i is the current density at the corresponding point. The potential distribution on the surface of the sample reflects the current accumulation at each point.

(2) Measurement of piezoelectric constant

A load of 150 g is periodically applied to the sample, and the electrical response generated in the sample is recorded by an electrometer after passing through the signal amplifier. The relationship between the force F=mg generated by the load, the charge Q accumulated on the electrode during the load and the longitudinal piezoelectric constant d33 can be expressed as:

ISSN 2616-5880 Vol. 4, Issue 5: 61-70, DOI: 10.25236/AJMC.2023.040509

$$d_{33} = Q / F \tag{8}$$

(3) Electric field force microscope measurement method

Assuming that the thickness of the sample is sufficiently small (L<<z0,z0 is the Rayleigh length of the Gaussian beam), the change in beam radius due to diffraction or refractive index changes in the sample is negligible. Under this approximation, the nonlinear absorption is negligible, and the normalized transmittance observed by electric field force microscopy can be expressed as:

$$T(z,\ \ \Delta\Phi_0(t)) = 1 + \frac{4\langle\Delta\Phi_0(t)\rangle \cdot x}{(x^2+9)(x^2+1)},\quad x = z / z_0$$
$$\Delta\Phi_0(t) = k\gamma I_0(t) L_{eff} \tag{9}$$

Where $\langle\Delta\Phi_0\rangle$ is the time average of the phase change at the optical axis focus; z is the distance between the sample and the focus, $z_0 = k\omega_0^2 / 2$ is the Rayleigh length of the beam; I0(t) is the illumination intensity at the focus of the laser beam; L is the sample The actual thickness (the thickness of the quartz dish used in the experiment), and $L_{eff} = (1 - e^{-aL}) / \alpha$ is the effective thickness of the sample, where α is the linear absorption coefficient of the sample; k is the wave vector; γ is the third-order nonlinear refractive index coefficient of the sample.

5. Results and Discussion

5.1. Charge Storage Performance Analysis of PVP Molecular Motion

In Figure 1, the peak currents of the five polymer space charge peaks are very different from the initial carrier concentrations. We first analyze them from their molecular structure.

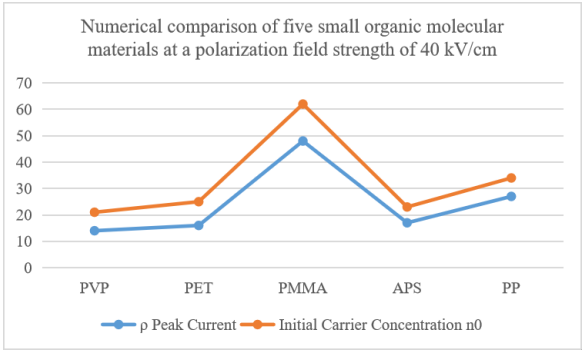

Figure 1: Comparison of peak current and initial carrier concentration of space charge peaks of five organic small molecular materials

The pendant pyrrolidone ring in the PVP molecule contains a lactam structure. If the polymer contains a polar group, each dipole of these polar groups can act as an electron or hole trap, thus a polar group-containing polymerization. The space charge trapped by traps is greatly increased. The strong polar lactam group in the PVP side group additionally captures a large amount of space charge. These space charges trapped in the trap are trapped under thermal stimulation and participate in the total conduction, causing the PVP electret to collapse under thermal stimulation. The amount of space charge is much larger than that of polymers with less polar side groups, so the space charge peak observed in this experiment is so large.

5.2. PVP Charge Storage Characteristics of Ge-doped Oxide Films

(1) Measurement and analysis of capacitance voltage curve

Figure 2 is a C-V plot of a Ge-doped film at different scan voltages.

ISSN 2616-5880 Vol. 4, Issue 5: 61-70, DOI: 10.25236/AJMC.2023.040509

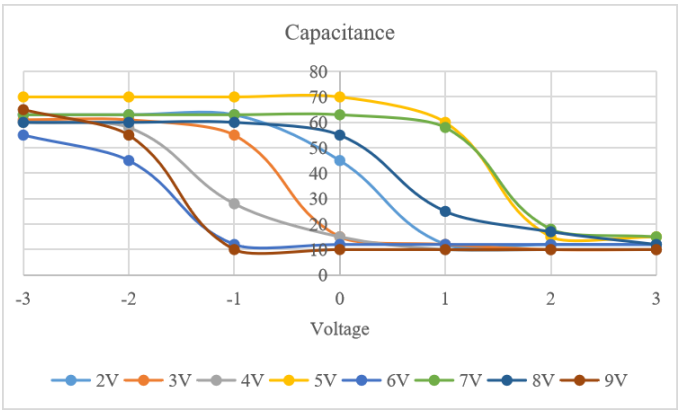

Figure 2: C-V curve of Ge-doped film under different scanning voltages.

The test mode is Cs-D, the scan voltage range is gradually increased from ±2 to ±9, the voltage scanning step size is 0.02V, and the C-V curve spectrum corrected by the dual-frequency method is shown in Figure 2. A counterclockwise hysteresis window was observed in the CV curves for different cyclic voltage sweeps because electrons in the channel tunneled through the thinner Ge oxide tunneling layer (about 4 nm) under high electric field and were incorporated into the Ge oxide film. The result of electrical mirroring resulting from the release of the atomic capture. As the scan voltage increases, the hysteresis window of the CV curve also increases gradually; when the scan voltage is ±2V, the flat-band voltage difference corresponding to the window is only about 0.8V; when the scan voltage is increased to ±6V, the hysteresis window width is reached. 3.0V. subsequently, although the scanning voltage is continuously increased, the window width remains almost unchanged. The possible reasons are as follows: When the PVP substrate is excessive from the inversion region to the deep depletion region, the PVP substrate can no longer provide more electron injection tunneling layer, and the Ge memory cell gradually becomes saturated due to the silo blockage effect, unable to store more injected electrons; therefore the storage window is no longer increased. On the other hand, when the scan voltage is increased to a certain value, the probability that the electrons stored in the Ge memory cell are lost through the gate control layer is gradually increased, and the dynamic balance between the two causes the CV curve hysteresis window width to finally reach Stable value.

(2) Charge storage aging performance

Figure 3 is a graph of the curve of the doped Ge oxide film and the percent charge loss as a function of test time.

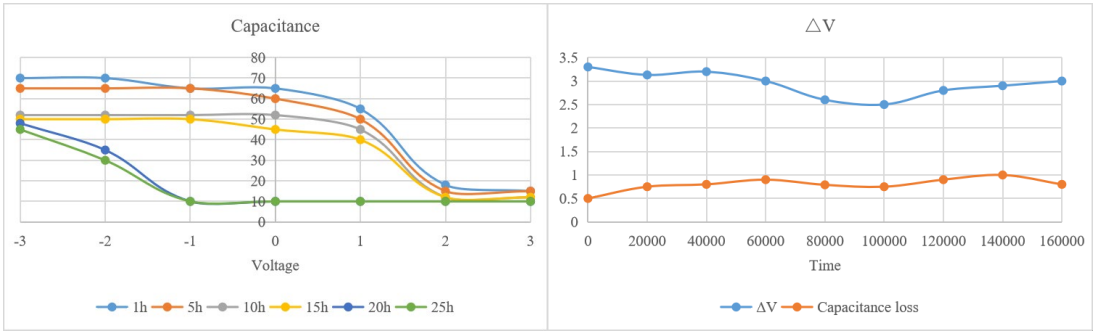

(a) C-V *(b) ΔV and percentage of charge loss*

Figure 3: Curve of the oxide-doped oxide film and the percentage of charge loss as a function of test time.

The CV hysteresis curve window width of the PVP device doped with Ge oxide film reflects the amount of charge storage, while the film accumulated state capacitance value reflects the dielectric properties of the film. The magnitude of the applied bias voltage Vg is the device withstands voltage. One of the performance parameters. As can be seen from Fig. 2, the flat-band voltage difference obtained when the scanning voltage is ±6 V is the largest. Therefore, only the aging performance of the Ge-doped oxide film under ±6 V gate voltage will be discussed later. Figure 3 shows a plot of C-V curve for a 30-hour continuous measurement of a thin-film device at ±6 V gate voltage, and a plot of charge-loss-time vs. flat-band voltage-time. After continuous measurement, the hysteresis window of CV curve fluctuates between 2.5 and 3.0V, and no obvious decay is observed. This fully demonstrates

ISSN 2616-5880 Vol. 4, Issue 5: 61-70, DOI: 10.25236/AJMC.2023.040509

that the stored charge in the device has good time-lasting performance. At the same time, the cumulative state capacitance of the film is Cmax. The size of the device is only slightly fluctuating with time, showing a very stable nature, which means that the capacitance decay (loss of charge) is very small and has good charge aging performance.

5.3. Effect of Substrate Temperature on PVP Charge Mobility

Figure 4 shows the transmission characteristics of a PVP device prepared at different substrate temperatures at a source-drain voltage of -60V, and the relationship between the square root of the source-drain current and the gate voltage. It can be seen from the transmission curve of the device that all devices have good saturation characteristics. With a certain source-drain voltage, the channel current will gradually increase with the increase of the gate voltage, at 340K temperature. The prepared PVP has the largest channel current, and the PVP channel current prepared at 360K is the smallest. By plotting the relationship between the square root of the device source-drain current and the gate voltage, we can fit the slope of the curve. It can be seen that the charge mobility of the device in the saturation region can be calculated from the slope of the straight line portion of the curve. Table 1 show that the dielectric constant of the silicon dioxide during the calculation was 11.9nF/cm2 and the channel aspect ratio of the device was 1:20.

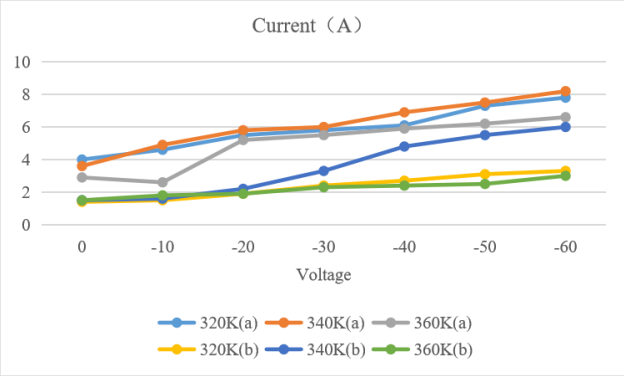

Figure 4: Transmission characteristics of a PVP device prepared at different substrate temperatures at a drain voltage of -60 V (a), the relationship between the square root of the source-drain current and the gate voltage (b).

Table 1: Charge mobility of PVP devices prepared at different substrate temperatures.

Substrate Temperature	Charge Mobility
320K	0.089
340K	0.21
360K	0.0103

It can be seen from the results in the table that as the substrate temperature increases the charge mobility of PVP increases first and then decreases. The PVP mobility prepared at 340K reaches 0.21 cm2/Vs, which is 360K. 18 times the performance of PVP prepared at temperature. The carrier mobility of the material is determined by the size of the semiconductor thin film particles and the distance between the particles. The larger the size of the thin film particles, the higher the mobility, and the larger the distance between the particles, the smaller the mobility. We believe that the PVP film formed at 340K has larger crystal grains and the distance between the crystal grains is relatively small, thus effectively reducing the loss of charge during transmission, resulting in relatively good device performance. By observing the morphology of the film at 320K and 360K, it can be found that although the grain sizes of the two are not much different, the film formation of the former is better than that of the latter, and the grain boundaries are smoother, resulting in higher Charge mobility. Based on the above analysis, we believe that the increase in substrate temperature will help improve the performance of PVP devices, but should not exceed 360K.

6. Conclusion

In order to further understand the complex electrical mechanism in organic small molecule thin film materials, improve device efficiency, lifetime and stability. In this paper, the electrical properties of

ISSN 2616-5880 Vol. 4, Issue 5: 61-70, DOI: 10.25236/AJMC.2023.040509

organic small molecule thin film materials were studied by electrostatic field force microscopy (EFM). When the temperature is lower than 100 °C, the PVP dielectric frequency spectrum can be decomposed into γ relaxation, β relaxation and DC conductivity. When the temperature is higher than 100 °C, the γ relaxation exceeds the frequency measurement range, and the complex dielectric coefficient of PVP can be decomposed into β relaxation and DC conductivity. After the temperature is higher than 130 °C, α relaxation occurs at low frequencies. We believe that an increase in substrate temperature will help improve the performance of PVP devices, but should not exceed 360K. This fully demonstrates that the stored charge in the device has good time-lasting performance. At the same time, the cumulative state capacitance value Cmax of the film has only a slight fluctuation with time, showing a very stable property, which indicates the capacitance decay (charge loss) very small, with good charge aging properties.

References

[1] Pandey, M., Joshi, G. M., Deshmukh, K., Ghosh, N. N., & Raj, N. A. N. (2015) "Electrical conductivity, optical properties and mechanical stability of 3, 4, 9, 10-perylenetetracarboxylic dianhidride based organic semiconductor", Journal of Physics and Chemistry of Solids, 80, pp.52-61.

[2] Han, Y., Ning, W., Cao, L., Xu, X., Li, T., Zhang, F. & Tian, M. (2016) "Photophysical and electrical properties of organic waveguide nanorods of perylene-3, 4, 9, 10-tetracarboxylic dianhydride", Nano Research, 9(7), pp. 1948-1955.

[3] Mahmood, J., Lee, E. K., Jung, M., Shin, D., Choi, H. J., Seo, J. M. & Park, N. (2016) "Two-dimensional polyaniline (C3N) from carbonized organic single crystals in solid state", Proceedings of the National Academy of Sciences, 113(27), pp.7414-7419.

[4] Salzmann, I., Heimel, G., Oehzelt, M., Winkler, S., & Koch, N. (2016) "Molecular electrical doping of organic semiconductors: fundamental mechanisms and emerging dopant design rules", Accounts of chemical research, 49(3), pp.370-378.

[5] Das, T., Das, B. K., Parashar, S. K. S., & Parashar, K. (2017) "Impact of divalent dopant Ca 2+ on the electrical properties of ZnO by impedance spectroscopy", Bulletin of Materials Science, 40(1), pp.247-251.

[6] Wang, L. G., Zhu, J. J., Liu, X. L., & Cheng, L. F. (2017) "Characterization of the Hole Transport and Electrical Properties in the Small-Molecule Organic Semiconductors", Journal of Electronic Materials, 46(10), pp.5546-5552.

[7] Adinolfi, V., Peng, W., Walters, G., Bakr, O. M., & Sargent, E. H. (2018) "The electrical and optical properties of organometal halide perovskites relevant to optoelectronic performance", Advanced Materials, 30(1), pp.1700764.

[8] Anitha, R., Vavilapalli, D. S., Menon, S. S., Surender, S., Baskar, K., & Singh, S. (2018) "Hybrid gallium nitride/organic heterojunction with improved electrical properties for optoelectronic applications", Journal of materials science, 53(16), pp. 11553-11561.

[9] Marrese, M., Guarino, V., & Ambrosio, L. (2017) "Atomic force microscopy: a powerful tool to address scaffold design in tissue engineering", Journal of functional biomaterials, 8(1), pp.7.

[10] Osayemwenre, G. O., Meyer, E. L., & Taziwa, R. T. (2018) "Investigation of Contact Potential Variation in Amorphous Silicon Module Interface by Scanning Kelvin Prob[e Microscopy", Advanced Science, Engineering and Medicine, 10(9), pp.870-875.

[11] Mu, S., Liu, Q., Kidkhunthod, P., Zhou, X., Wang, W., Tang, Y. (2020). Molecular grafting towards high-fraction active nanodots implanted in N-doped carbon for sodium dual-ion batteries. National science review, 8(7). doi: 10.1093/nsr/nwaa178

[12] X Xu, Karami, B., & Shahsavari, D. (2021). Time-dependent behavior of porous curved nanobeam. International Journal of Engineering Science, 160, 103455.

[13] Zhao, Y., & Kok Foong, L. (2022). Predicting electrical power output of combined cycle power plants using a novel artificial neural network optimized by electrostatic discharge algorithm. Measurement, 198, 111405. (doi: 10.1016/j.measurement. 2022.111405)

[14] Xiyue Cao, Jianfei Xia, Xuan Meng, Jiaoyan Xu, Qingyun Liu, Zonghua Wang. (2019) Stimuli-Responsive DNA-Gated Nanoscale Porous Carbon Derived from ZIF-8. Adv. Funct. Mater. 29, 1902237.

[15] Handelzalts Shirley. (2021) New Ferroelectric Material Technology in Remote Electrical Control System of Smart Home. Distributed Processing System, Vol. 2, Issue 1: 58-74.

[16] Zeng, L., Shi, J., Luo, J., & Chen, H. (2018) "Silver Sulfide Anchored on Reduced Graphene Oxide as A High-Performance Catalyst for CO2 Electroreduction", Journal of Power Sources, 398, pp. 83-90.